Research Article

Formation of a K—In—Se Surface Species by NaF/KF Postdeposition Treatment of Cu(In,Ga)Se₂ Thin-Film Solar Cell Absorbers

Evelyn Handick,[*,†] Patrick Reinhard,[‡] Regan G. Wilks,[†,§] Fabian Pianezzi,[‡] Thomas Kunze,[†] Dagmar Kreikemeyer-Lorenzo,[∥] Lothar Weinhardt,[∥,⊥] Monika Blum,[⊥] Wanli Yang,[#] Mihaela Gorgoi,[§,∇] Eiji Ikenaga,[○] Dominic Gerlach,[◆] Shigenori Ueda,[¶,▲] Yoshiyuki Yamashita,[◆] Toyohiro Chikyow,[◆] Clemens Heske,[∥,⊥] Stephan Buecheler,[‡] Ayodhya N. Tiwari,[‡] and Marcus Bär[*,†,§,⬡]

[†]Renewable Energy, Helmholtz-Zentrum Berlin für Materialien und Energie GmbH (HZB), Hahn-Meitner Platz 1, 14109 Berlin, Germany

[‡]Laboratory of Thin Films and Photovoltaics, Empa-Swiss Federal Laboratories for Materials and Science and Technology, Überlandstraße 129, 8600 Dübendorf, Switzerland

[§]Energy Materials In-Situ Laboratory Berlin, Helmholtz-Zentrum Berlin für Materialien und Energie GmbH, Albert-Einstein-Straße 15, 12489 Berlin, Germany

[∥]Institute for Photon Science and Synchrotron Radiation (IPS) and Institute for Chemical Technology and Polymer Chemistry (ITCP), Karlsruhe Institute of Technology (KIT), Hermann-von-Helmholtz-Platz 1, 76344 Eggenstein-Leopoldshafen, Germany

[⊥]Department of Chemistry and Biochemistry, University of Nevada, Las Vegas (UNLV), 4505 S. Maryland Parkway, Las Vegas, Nevada 89154-4003, United States

[#]Advanced Light Source (ALS), Lawrence Berkeley National Laboratory, 1 Cyclotron Road, Berkeley, California 94720, United States

[∇]Institute for Nanospectroscopy, Helmholtz-Zentrum Berlin für Materialien und Energie GmbH, Albert-Einstein-Straße 15, 12489 Berlin, Germany

[○]SPring-8/JASRI, 1-1-1 Koto, Sayo-cho, Hyogo 679-5198, Japan

[◆]MANA/Nano-Electronics Materials Unit, National Institute for Materials Science, 1-1 Namiki, Tsukuba, Ibaraki 305-0044, Japan

[¶]Synchrotron X-ray Station at SPring-8, NIMS. 1-1-1 Kouto, Sayo-cho, Hyogo 679-5148, Japan

[▲]Quantum Beam Unit, NIMS, 1-2-1, Sengen, Tsukuba, Ibaraki 305-0047, Japan

[⬡]Institut für Physik und Chemie, Brandenburgische Technische Universität Cottbus-Senftenberg, Platz der Deutschen Einheit 1, 03046 Cottbus, Germany

S *Supporting Information*

ABSTRACT: A NaF/KF postdeposition treatment (PDT) has recently been employed to achieve new record efficiencies of Cu(In,Ga)Se₂ (CIGSe) thin film solar cells. We have used a combination of depth-dependent soft and hard X-ray photoelectron spectroscopy as well as soft X-ray absorption and emission spectroscopy to gain detailed insight into the chemical structure of the CIGSe surface and how it is changed by different PDTs. Alkali-free CIGSe, NaF-PDT CIGSe, and NaF/KF-PDT CIGSe absorbers grown by low-temperature coevaporation have been interrogated. We find that the alkali-free and NaF-PDT CIGSe surfaces both display the well-known Cu-poor CIGSe chemical surface structure. The NaF/KF-PDT, however, leads to the formation of bilayer structure in which a K—In—Se species covers the CIGSe compound that in composition is identical to the chalcopyrite structure of the alkali-free and NaF-PDT absorber.

KEYWORDS: chalcopyrite thin-film solar cells, alkali postdeposition treatment, photoelectron spectroscopy, X-ray spectroscopy, chemical surface structure
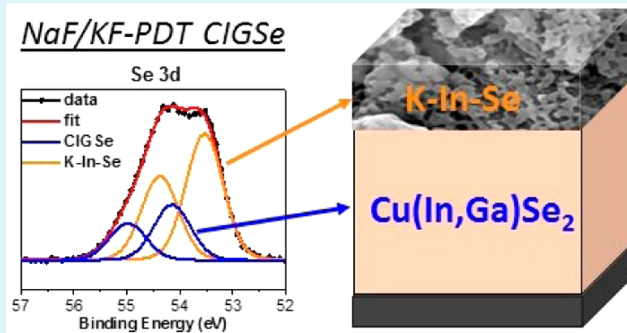
■ INTRODUCTION

A recent boost in record efficiencies for Cu(In,Ga)Se₂ (CIGSe)-based solar cells (with efficiencies exceeding 22%[1,2])

was brought about using NaF and/or KF postdeposition treatments (PDTs).[3,4] It is well established that sodium diffusion from the underlying soda lime glass substrate (or the deliberate introduction of a Na-containing precursor[5]) is necessary for good efficiencies.[5−8] Furthermore, recent records have been achieved with an additional incorporation of alkali elements (such as, e.g., potassium) in the absorber by a postdeposition treatment using alkali fluorides.[3,4] Even though this breakthrough is closely related to providing potassium during[9] or after[3,4] the absorber formation, the underlying mechanism of its beneficial role in modifying the chemical, electronic, and/or topographical[10] absorber properties has not yet been fully understood.

It has been reported that a NaF/KF-PDT can result in a "nanopatterned" CIGSe surface topography.[11] In addition, it impacts the chemical structure at the absorber surface, notably causing copper and gallium depletion after the deposition of K.[4,11] The electronic structure of the surface is also influenced, leading to an unprecedented band gap widening in the near-surface (K-containing and Cu- and Ga-depleted) region, up to 2.52 (+0.14/-0.51) eV.[11] As a result, it has been speculated that a K—In—Se-type surface phase is formed.[11−13]

To study the chemical structure and derive insights into the underlying mechanism for the significant performance improvement of the NaF/KF-PDT, we have used lab- and synchrotron-based X-ray photoelectron spectroscopy (XPS) to determine the surface composition (profile) of an untreated (i.e., alkali-free), a NaF-PDT, and a NaF/KF-PDT CIGSe absorber. To further elucidate the specific chemical environment of potassium and selenium, synchrotron-based X-ray emission (XES), and X-ray absorption spectroscopy (XAS) were used to provide element-specific information about the partial densities of occupied and unoccupied states, respectively.

■ EXPERIMENTAL SECTION

The samples were prepared by Empa using a low-temperature multistage process.[4] CIGSe absorbers were deposited onto flexible polyimide foils coated with molybdenum. The as-prepared alkali-free CIGSe absorbers were treated with a postdeposition treatment (PDT) of NaF or NaF/KF according to ref 4. Similarly prepared solar cell devices by Empa reached efficiencies of 18.7%[14] and 20.4%.[4] A K—In—Se reference sample was prepared on a soda lime glass substrate with a diffusion barrier and a Mo layer by evaporating an In_2Se_3 layer, followed by coevaporation of KF and Se at a similar substrate temperature as during PDT. However, the KF evaporation rate was increased (4−8 nm/min) compared to the NaF/KF-PDT CIGSe process (1−2 nm/min), with an accordingly adjusted Se flux and the duration was increased from 20 to 60 min. Excess KF was dissolved with water, resulting in a final K content of 13.7 at% in the indium selenide precursor, as measured by inductively coupled plasma mass spectrometry. This reference sample will be called "KF-PDT In_2Se_3" hereafter. To prevent surface contamination and minimize air exposure, all samples were sealed and packed in a N_2-filled glovebag attached to the deposition chamber at Empa, and opened in a N_2-filled glovebox attached to the ultrahigh vacuum (UHV) surface analysis system at HZB. To remove alkali fluoride residue from the surface of the PDT samples, they were immersed in aqueous ammonia solution (1 mol/L) for 1−2 min outside the glovebox and rinsed/stored in deionized (DI) H_2O until reintroduction into the glovebox via the load lock chamber (in which they were vacuum-dried). The KF-PDT In_2Se_3 sample was only washed in DI water. No further cleaning (e.g., by Ar^+ sputtering) of the sample surface was performed before measurements.

Lab-based XPS measurements were conducted using nonmonochromatized Mg K_α (1253.56 eV) and Al K_α (1486.58 eV) radiation and a SPECS PHOIBOS 150 MCD-9 electron energy analyzer. The base pressure of the analysis chamber was $<3 \times 10^{-10}$ mbar. The electron energy analyzer was calibrated according to D. Briggs et al.[15] For the collection of the (shallow) core levels and Auger lines, the pass energy was set to 30 eV, resulting in a combined resolution for XPS measurements of approximately 1 eV.

Synchrotron-based hard X-ray photoelectron spectroscopy (HAXPES) experiments with excitation energies of 2, 6, and 8 keV were conducted at the HiKE end-station[16] (2 keV) on the KMC-1 beamline[17] of the BESSY II electron storage ring, and at beamlines BL15XU[18,19] (6 keV) and BL47XU[20] (8 keV) of the SPring-8 electron storage ring. For the SPring-8 measurements, the samples were only briefly exposed to air (<5 min), while for the 2 keV measurements the air exposure of the samples was significantly longer (a few hours). For the alkali-free CIGSe sample, we identified a minor Zn surface contamination for 2 and 8 keV (see Supporting Information Figure S1, center and bottom spectra) after storage in a different UHV system. The base pressure at the HiKE and BL47XU HAXPES end-stations was $<1 \times 10^{-8}$ mbar, and better than 1×10^{-9} mbar at BL15XU; all are equipped with a Scienta R4000 hemispherical electron energy analyzer with similar setups for beamline and analyzer. The beamlines are equipped with double crystal monochromators (DCMs), allowing to tune the excitation energy between 2.0 and 10.0 keV at KMC-1, 2.2 and 36.0 keV at BL15XU, and between 5.2 and 37.7 keV at BL47XU. A pass energy of 200 eV was used for all measurements, and the excitation energy was calibrated by measuring multiple 4f spectra of a grounded clean Au foil and setting the Au $4f_{7/2}$ binding energy equal to 84.00 eV.[21] Spectra were recorded using photon energies of 2 keV at BESSY II and of 6 and 8 keV at SPring-8 using the first, third, and fourth reflection order of the Si(111) DCM crystal, providing combined analyzer plus beamline total energy resolution of approximately 0.25 eV for all HAXPES spectra.

The relative composition of the samples was determined by fitting the XPS and HAXPES spectra of the respective shallow core levels with Voigt profiles and a linear background, and by taking the respective photoionization cross sections[22,23] into account (see description of Figure S2 for more details). Using different excitation energies will result in different kinetic energies and thus different inelastic mean free paths (IMFPs) of the emitted photoelectrons,[24] allowing to derive a "depth-dependent" composition.

Synchrotron-based soft X-ray emission (XES) and absorption (XAS) spectroscopy were performed in the soft X-ray fluorescence (SXF) endstation[25] of ALS beamline 8.0.1. The samples were transferred into the chamber after only a short air-exposure. Photon energies of 120 eV and a range of 280−306 eV were used for Se $M_{4,5}$ XES and K $L_{2,3}$ XAS measurements, respectively. The XES energy scale was calibrated using elastically scattered photons in the range of 100−120 eV in second diffraction order of the spectrometer. XAS spectra were recorded in the total fluorescence yield mode using a channeltron detector, and for excitation energy calibration, a C K absorption spectrum of HOPG (highly oriented pyrolytic graphite) was measured (see Figure S6).

■ RESULTS AND DISCUSSION

In order to derive a "depth-dependent" picture of the composition of the differently treated CIGSe absorber surfaces, and relate the them to the findings on the electronic structure in ref 11, we characterized the samples by photoelectron spectroscopy using different excitation energies (Mg K_α and 2, 6, and 8 keV). This results in a variation of the inelastic mean free path (IMFP) of the photoelectrons from approximately 3 nm to a maximum of 12 nm for the shallow core levels.[24] To derive the sample surface composition at each photon energy, we have exclusively used the intensity of the shallow core levels Cu 3p, Se 3d, Ga 3d, In 4d, and K 3s. They have similarly low binding energies and thus comparable high kinetic energies (between 1180−1240 eV for Mg K_α, 1925−1990 eV for 2 keV, 5875−5940 eV for 6 keV, and 7865−7930 eV for 8 keV). This allows us to neglect the impact of variations in IMFP and
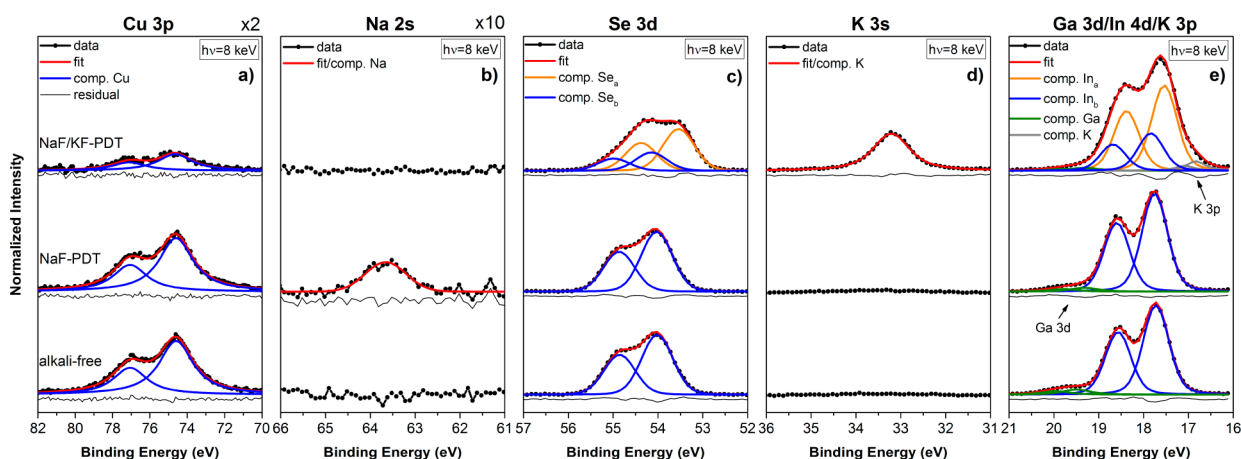
Figure 1. HAXPES data of alkali-free (bottom), NaF-PDT (center), and NaF/KF-PDT (top) CIGSe samples, recorded with an excitation energy of $h\nu = 8$ keV: Cu 3p (a), Na 2s (b), Se 3d (c), K 3s (d), and Ga 3d/In 4d/K 3p (e). The respective fits with Voigt profiles (doublets) and the residuals of the fits are also displayed. All spectra are displayed area-normalized to the Se 3d peak area and shown with the respective linear background subtracted. For better visibility, the Cu 3p and Na 2s spectra are magnified by a factor of ×2 and ×10, respectively.
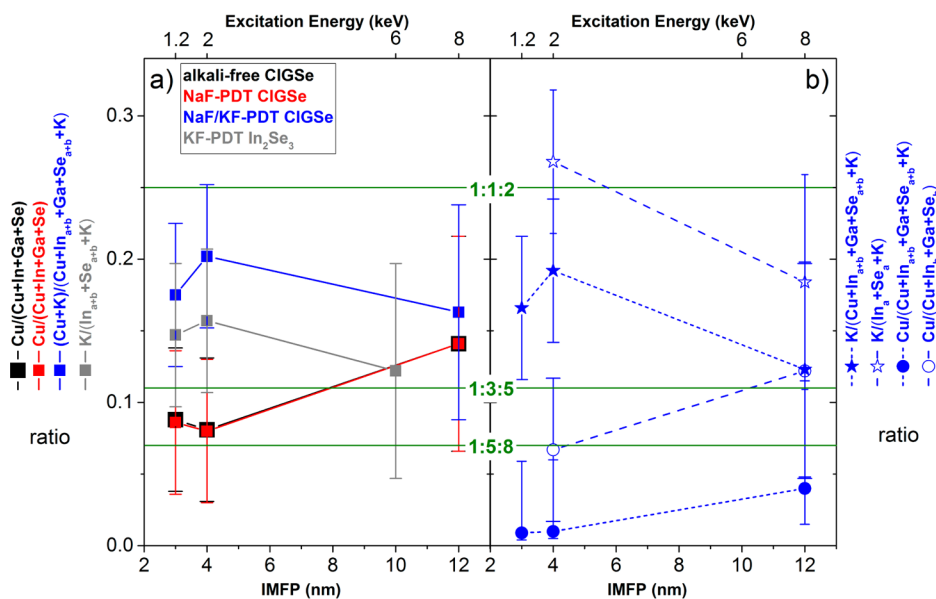
Figure 2. (a) (Cu+K)/(Cu+In+Ga+Se+K) ratios of differently treated Cu(In,Ga)Se$_2$ (CIGSe) absorbers, taken with Mg K$_\alpha$ and 2, 6, and 8 keV excitation (resulting in IMFPs of 3, 4, 10, and 12 nm).[24] Black: alkali-free CIGSe; Red: NaF postdeposition treatment (PDT) CIGSe; Blue: NaF/KF-PDT CIGSe. For reference, the composition of a KF-PDT In$_2$Se$_3$ (gray) sample is also shown. (b) Individual Cu/(Cu+In$_{a+b}$+Ga+Se$_{a+b}$+K) and K/(Cu+In$_{a+b}$+Ga+Se$_{a+b}$+K) ratios (short dashed blue lines, filled symbol), as well as Cu/(Cu+In$_b$+Ga+Se$_b$) and K/(K+In$_a$+Se$_a$) ratios (long dashed blue lines, open symbols) for the NaF/KF-PDT CIGSe sample. In$_a$ & Se$_a$ and In$_b$ & Se$_b$ represent the spectral contributions ascribed to a K—In—Se species and the chalcopyrite absorber, respectively (see Figure 1). The most common nominal CIGSe-related stoichiometries ([Cu+K]:[In+Ga]: [Se] = 1:1:2, 1:3:5, and 1:5:8) are depicted in green. A general error margin of ±0.05 eV for Mg K$_\alpha$ and 2 keV, and ±0.075 eV for 6 and 8 keV, is assumed.

electron analyzer transmission for each data set. Furthermore, for each excitation energy, the shallow core level peaks are similarly attenuated by surface adsorbates. This is an important consideration for the current data set, as oxygen and carbon are detected on all investigated samples, even for the more bulk sensitive (i.e., 6 and 8 keV) measurements, indicating a pronounced contamination layer at the sample surfaces. Furthermore, C and/or O incorporation into the absorber bulk can also not be ruled out.

Figure 1 shows the Cu 3p (corrected by the In 4p background, see Figure S5 for more details), Na 2s, Se 3d, K 3s, and Ga 3d/In 4d/K 3p core-level HAXPES spectra taken at 8 keV for all CIGSe samples. The individual photoemission

lines were fitted simultaneously (see Figure S3 and ref 26 for more details). All peaks can be fitted reasonably well with one species (note that the p and d lines are composed of a doublet), except for the Se 3d and In 4d spectra for the NaF/KF-PDT CIGSe sample. For these photoemission lines, (at least) two contributions (a and b) were needed for a satisfactory description.

As expected, potassium (K 3s and K 3p) is only seen on the NaF/KF-PDT CIGSe sample. Conversely, appreciable Ga 3d lines are only detected on the alkali-free and NaF-PDT CIGSe samples. However, note that the most prominent Ga core level (Ga 2p) can also be identified and significantly increases with photon energy (i.e., with decreasing surface sensitivity) for the

NaF/KF-PDT CIGSe sample (see Figure S1). Nevertheless, we tentatively attribute the second contribution to the Se 3d and In 4d photoemission lines at low binding energies (Se$_a$ 3d$_{5/2}$: 53.54 eV; In$_a$ 4d$_{5/2}$: 17.53 eV) to a K—In—Se surface species. This attribution naturally implies that the high binding energy contributions (Se$_b$ 3d$_{5/2}$: 54.15 eV; In$_b$ 4d$_{5/2}$: 17.83 eV) represent the chalcopyrite absorber; the binding energies of these components are in agreement with the equivalent binding energies in the alkali-free (Se 3d$_{5/2}$: 54.02 eV; In 4d$_{5/2}$: 17.72 eV) and NaF-PDT (Se 3d$_{5/2}$: 54.03 eV; In 4d$_{5/2}$: 17.75 eV) case. Note that the experimental uncertainty for all stated binding energies is (± 0.10) eV.

From the fits of the photoemission data (see Figure 1, Figures S1 and S4, and ref 26 for all of the data and more analysis details), we can derive relative Cu/(Cu+In+Ga+Se) ratios for the alkali-free and NaF-PDT CIGSe samples, and a respective (Cu+K)/(Cu+K+In$_{a+b}$+Ga+Se$_{a+b}$) ratio for NaF/KF-PDT CIGSe, which represents partial occupation of Cu by K,[27] as a function of employed excitation energy (and thus as a function of IMFP). The subscripts "a" and "b" refer to the K—In—Se and CIGSe components in the In 4d and Se 3d photoemission lines of the NaF/KF-PDT CIGSe sample, respectively. The results are displayed in Figure 2. The signal intensity is related to the relative quantity of the respective element in the probed sample volume, weighted exponentially according to the IMFP. As such, for materials with an uniform composition throughout the investigated volume, the obtained composition results reflect the true (uniform) composition. For a nonuniform material, the values will additionally be influenced by the depth-dependence of the composition. By employing a broad range of photon energies, this additional influence can be exploited. Note that the error margin indicated in Figure 2 is dominated by the uncertainty of the photoionization cross section correction and thus represents the absolute uncertainty of the quantification of the photo-emission data. In the following, we will discuss relative changes, for which the uncertainty is significantly lower.

We assume that the C and O contaminants mainly reside on the surface, and thus do not include them in the compositional analysis. Additionally, Na is neglected from further analysis, as the amount of Na found for the NaF-PDT CIGSe is low compared to the K concentration observed for the NaF/KF-PDT CIGSe sample (less than 10% for the 8 keV measurements). The (Cu)/(Cu+In+Ga+Se) ratios of the alkali-free and NaF-treated CIGSe are very similar, suggesting that the Zn contamination observed for the alkali-free CIGSe sample (see discussion above and Figure S1) does not have a large influence on the determined ratios. Compared to the nominal bulk stoichiometry of Cu:(In+Ga):Se = 1:1:2, the ratios that represent the most surface-sensitive measurements in Figure 2a (and in Figure S5) for both absorber samples are consistent with Cu-poor chalcopyrite structures (having a surface stoichiometry of 1:3:5 or 1:5:8). Such Cu-deficient surfaces have been reported for high-efficiency chalcopyrites before,[28,29] and have been attributed to the formation of ordered defect/vacancy surface compounds[30,31] or surface reconstruction.[32] The more bulk-sensitive 8 keV data shows an increasing Cu content, confirming that the Cu-deficiency is most pronounced at the absorber surface.

The surface of the NaF/KF-treated CIGSe has significantly less Cu than the alkali-free or NaF-PDT CIGSe samples, as was reported in refs 4 and 11. However, the Cu signal becomes significant in the 8 keV HAXPES (IMFP of approximately 12

nm) data of this sample (see Figure 1a), suggesting that deeper beneath the surface, the derived Cu content approaches that observed at the surfaces (i.e., within the first few nm) of the alkali-free and NaF-PDT CIGSe samples (see Mg K$_\alpha$ and 2 keV data, see Figure 2). Furthermore, a significant amount of K is found on the NaF/KF-PDT CIGSe surface (see Figure 1d, and refs 4 and 11), as indicated by the respective K/(Cu+In$_{a+b}$+Ga+Se$_{a+b}$+K) profile in Figure 2b. The trend in K content is mainly opposite to that of the Cu content [see Cu/(Cu+In$_{a+b}$+Ga+Se$_{a+b}$+K)], i.e., the concentration decreases with increasing bulk sensitivity. On the basis of DFT calculations, Ghorbani et al. suggest that K preferentially occupies Cu vacancies in a Cu-poor CIGSe material.[27] This model correlates well with the previous finding that the electronic surface structure of this set of NaF/KF-PDT CIGSe absorbers[11] is in agreement with the formation of a K—In—Se surface compound. In Figure 2a), we therefore include a curve (blue, filled squared symbols) showing the composition of an assumed (Cu,K)-(In,Ga)-Se [i.e., (Cu+K)/(Cu+In$_{a+b}$+Ga+Se$_{a+b}$+K)] species, in which K occupies a certain number of Cu vacancies. Note that for the NaF/KF-PDT sample only a neglible amount of Ga is found at the very surface (see Figure S1 top and center; a significant amount of Ga is only found in the 8 keV data, see Figure S1). When the Cu and K contributions are combined in this way, the composition tends away from the Cu-poor structures and toward the stoichiometric 1:1:2 composition. This stoichiometry is also confirmed by the Se content shown in Figure S5b, blue filled squares. However, the (In+Ga) amount rather indicates a higher composition ratio compared to the 1:1:2 stoichiometry (see Figure S5a, blue filled symbols). Note that these conclusions could be impacted by the large experimental uncertainty.

As a reference, we also studied an In$_2$Se$_3$ thin film that was subjected to a KF-PDT (note that no combined NaF/KF-PDT was performed in this case). The corresponding K/(K+In$_{a+b}$+Se$_{a+b}$) ratio is depicted in Figure 2a. The derived potassium amount is lower than what is expected for a stoichiometric KInSe$_2$. Thus, the formation of a KInSe$_2$−In$_2$Se$_3$ mixture and/or a K-deficient K—In—Se species is proposed. The K/(Cu+In$_{a+b}$+Ga+Se$_{a+b}$+K) ratio (Figure 2b, blue solid stars) of the NaF/KF-PDT CIGSe sample appears to follow a similar trend but is—despite agreeing within the experimental uncertainty—higher for all excitation energies, possibly as a result of the different PDT parameters. The K/(K+In$_a$+Se$_a$) ratio for the NaF/KF-PDT sample (blue open stars in Figure 2b) tends to a more stoichiometric KInSe$_2$ species, but also agrees with a proposed K-deficient K—In—Se species for the 8 keV data. Note that the Cu/(Cu+In$_b$+Ga+Se$_b$) ratio of the NaF/KF-PDT CIGSe sample (Figure 2b, blue open dots) is similar to that of the potassium-free absorbers (black and red squares in Figure 2a). However, there is less agreement between the (In+Ga)/(Cu+In$_b$+Ga+Se$_b$) and Se/(Cu+In$_b$+Ga+Se$_b$) ratios of the NaF/KF-PDT CIGSe sample (see S.I. Figure S5, blue open dots) and those of the alkali-free absorbers (see S.I. Figure S5, black and red squares). They only agree within the large experimental uncertainty. As discussed above, the values in Figure 2 arise from an integration of the composition of the investigated volume. However, the Cu-composition clearly depends on the IMFP (e.g., the surface of the NaF/KF-PDT CIGSe is nearly Cu free, as shown by the blue filled dots in Figure 2b), which directly indicates a nonuniform composition profile. This may be related to the nanopatterned surface of the sample (reported in ref 10 and

also observed in the current study), or may also indicate a composition gradient or bilayer structure. On the basis of our data alone, a distinction between these scenarios is very challenging. Furthermore, we note the uncertainty in determining the corresponding photoionization cross sections (see Figure S2).

To more directly examine the chemical speciation of the surfaces of the alkali-free, NaF-PDT, and NaF/KF-PDT CIGSe samples, the modified Auger parameter (α') of selenium $\alpha'(Se)$ = $E^b_{Se\ 3d_{5/2}} + E^k_{Se\ LMM}$ and indium $\alpha'(In) = E^b_{In\ 3d_{5/2}} + E^k_{In\ MNN}$ were calculated. The values for binding energy (E^b), Auger kinetic energy (E^k), and α' are shown in Figure 3 (the values
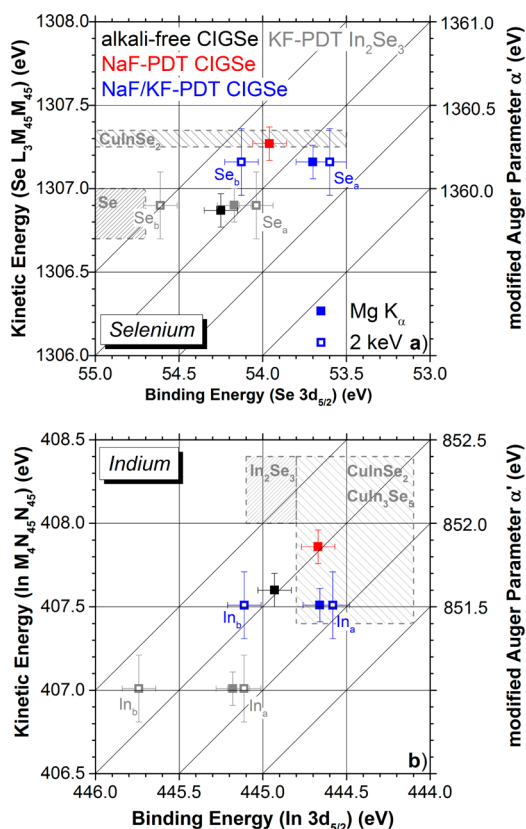
Figure 3. Wagner plots of the modified Auger parameter α' = $E^b_{core} + E^k_{Auger}$ for selenium (a) and indium (b), as derived for the alkali-free, NaF-PDT, NaF/KF-PDT CIGSe samples, and the KF-PDT In_2Se_3 reference. The filled symbols indicate measurements taken with Mg K_α and Al K_α excitation, while the open symbols are based on the 2 keV data for In $3d_{5/2}$ and Se $3d_{5/2}$ and the Auger kinetic energy derived with Mg K_α and Al K_α. The error margin is ± 0.1 eV for Mg K_α and Al K_α in x- and y-direction, as well as ± 0.1 eV in x and ± 0.2 eV in y-direction for the 2 keV data points.

used in the calculations can be found in Table S1). Independent of variations in doping concentration, (surface) band bending, and sample charging, chemically similar environments of the respective elements have the same modified Auger parameter α' and are located along diagonals within the Wagner-plot. The shaded boxes indicate the extent of binding and Auger kinetic energies for reference compounds reported in literature[33−42] and thus represent the largest possible spread of modified Auger parameters.

For the alkali-free (black) and the NaF-PDT (red) CIGSe, α' is very similar for both In and Se (i.e., the data can be found close to the same diagonal lines) suggesting—as did the

composition analysis above—that the chemical composition of their surfaces is similar. For the NaF/KF-PDT CIGSe (blue), the derived value for $\alpha'(Se)$ is slightly lower than for the alkali-free and NaF-PDT CIGSe; the overall variation in $\alpha'(Se)$ is, however, rather small, as expected for a sample set of selenides.[37] The $\alpha'(In)$ value of the NaF/KF-PDT CIGSe is similar to that of the KF-PDT In_2Se_3 sample (gray), confirming a similar chemical structure for these two samples—again in agreement with the analysis above.

For computing the modified Auger parameter α' (filled symbols), the laboratory-based XPS (Mg K_α and Al K_α, see Figure S4 [top panels]) data were used, in which—in contrast to the synchrotron data in Figure 1 and Figure S4 (bottom panels)—only one species for Se and In can be resolved for all samples. In order to also make use of the higher resolved HAXPES data, Figure 3 also includes data points (open symbols) that combine the 2 keV deduced E^b data with the respective Auger Mg K_α/Al K_α kinetic energy data. Note that for the thus-derived "approximated modified Auger parameters" two completely independent energy scales (the HAXPES E^b scale of the core levels and the XPS E^k scale of the Auger lines) are connected and thus are no longer inherently independent of variations in doping concentration, surface band bending, and/ or charging. The K—In—Se surface species (In_a and Se_a) located at lower binding energy has approximately the same $\alpha'(In)$ and $\alpha'(Se)$ for NaF/KF-PDT CIGSe (blue open squares in Figure 3) and KF-PDT In_2Se_3 (gray open squares in Figure 3). The CIGSe-species (In_b and Se_b) for the NaF/KF-PDT sample located at higher binding energy is similar to $\alpha'(In)$ and $\alpha'(Se)$ of the alkali-free and NaF-PDT CIGSe. The In—Se species (In_b and Se_b) for KF-PDT In_2Se_3 is shifted further to higher binding energies and toward an $\alpha'(In)$ representing an In_2Se_3 environment. However, note that there is significant deviation in binding and Auger kinetic energy compared to the reported values in literature, possibly caused by a different position of the Fermi level within the band gap due to (thickness dependent[43]) differences in optoelectronic properties.

The potassium and carbon Auger lines overlap, and thus deriving a meaningful modified Auger parameter for potassium is almost impossible. Hence, we carried out K $L_{2,3}$ XAS measurements (displayed in Figure 4) to probe the chemical environment of potassium in more detail. The nearby C K-edge XAS signal also contributes a significant background intensity for the potassium XAS measurements, but there are no prominent carbon-related peak structures in this region (see Figure S6). The C K-edge XAS spectrum of a highly order pyrolytic graphite (HOPG) sample was used for energy calibration and background consideration. The K $L_{2,3}$ XAS spectrum of the NaF/KF-PDT CIGSe sample is compared to that of the KF-PDT In_2Se_3 and a KF powder reference sample. As expected, no K $L_{2,3}$ absorption edge is observed for the NaF-PDT sample (see Figure S6).

The K $L_{2,3}$ XAS spectrum of the NaF/KF-PDT CIGSe sample resembles that of the KF-PDT In_2Se_3 reference, and both significantly differ from the spectrum of the KF-powder reference. The latter exhibits four sharp peaks (as found for all potassium halides[44,45]), split into two pairs (I, II and I′, II′). The splitting between L_2 and L_3, i.e., I and I′ as well as II and II′, is due to the spin−orbit splitting of the 2p states, while the splitting between I and II (as well as I′ and II′) is due to crystal field effects.[44−46] The absence of the distinct features (I, II and I′, II′) from the spectra of NaF/KF-PDT CIGSe and KF-PDT
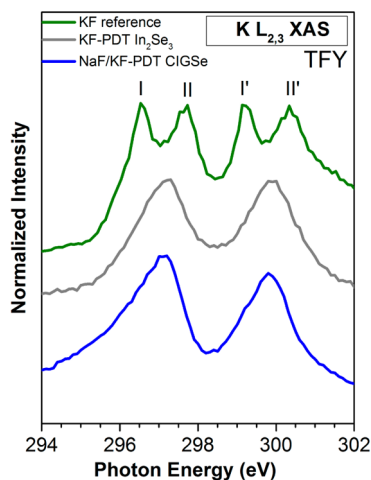
Figure 4. Potassium $L_{2,3}$ X-ray absorption spectra, measured in total fluorescence yield (TFY) mode, of the NaF/KF-PDT CIGSe sample (blue), in comparison to the KF-PDT In_2Se_3 reference (gray) and a KF powder reference (green).

In_2Se_3 indicates that there is little (if any) unreacted KF present after the PDT and rinsing procedures, as already suggested by ref 47. However, from the spectral resemblance of the K $L_{2,3}$ XAS spectrum of the NaF/KF-PDT CIGSe sample and the KF-PDT In2Se3 sample alone, it cannot unambiguously be concluded that the potassium is in a similar chemical environment, since both spectra also resemble K $L_{2,3}$ XAS data of K/GaAs[48] and K/Si.[49,50]

Hence, to further analyze the formation of a K—In—Se surface species, we directly examine the impact of the different PDTs on the local electronic structure near the Se atoms (including the hybridization of Se- and alkali-derived valence

states) using Se $M_{4,5}$ XES (Figure 5). This emission line gives information about the local partial density of occupied states (PDOS) as projected onto the Se 3d core hole. The spectra of the alkali-free (black) and the NaF-PDT CIGSe (red) absorbers in Figure 5a are effectively identical, indicating that there is no difference in the chemical environment of selenium in these samples (in agreement with our α'(Se)-related discussion above). The two K-containing samples, however, differ clearly from those without potassium, most clearly in the presence of an additional emission feature centered around 50 eV. The spectrum of a (powder) In_2Se_3 reference sample is also shown for comparison; it clearly deviates in shape from the spectra of the CIGSe absorbers as well as from that of the KF-PDT In_2Se_3 sample.

Figure 5b compares the spectral shape of the Se $M_{4,5}$ XES for the NaF/KF-PDT CIGSe sample with those of the reference samples in order to understand the chemical structure in more detail. As seen in the figure, the spectrum for NaF/KF-PDT CIGSe sample is reproduced by a simple two-component fit with the spectra of the NaF-PDT CIGSe and the KF-PDT In_2Se_3 samples. The fit results in a weight distribution of 0.5/0.5 for the two components. Note that no contribution from the In_2Se_3 powder reference sample is needed to reproduce the spectrum of NaF/KF-PDT CIGSe sample (see Figure S8). This result indicates the formation of a K—In—Se surface species on the NaF/KF-PDT CIGSe sample. The element-specific PDOS information obtained from the Se $M_{4,5}$ XES shown in Figure 5c is complementary to valence band photoemission taken from ref 11, as becomes apparent by direct comparison with "artificial HAXPES-derived XES spectra" displayed in Figure 5d. These spectra were derived by a superposition of two corresponding 8 keV photoemission valence band spectra, been offset by the Se $3d_{3/2}$ and $3d_{5/2}$ doublet separation of 0.83
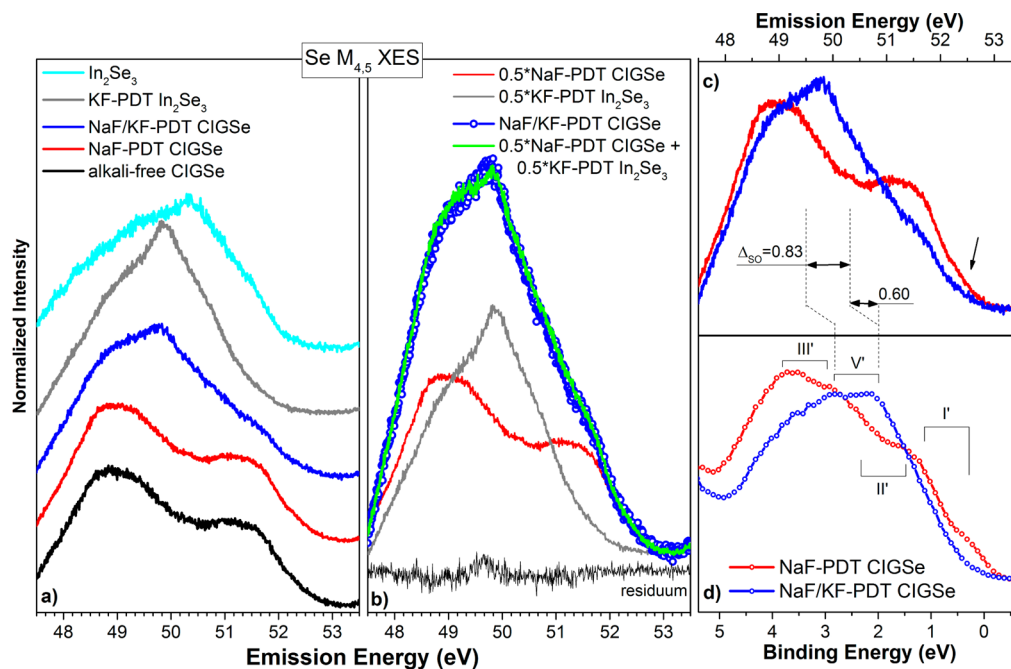
Figure 5. (a) Se $M_{4,5}$ XES spectra of the different Cu(In,Ga)Se$_2$ absorbers, compared to those of KF-PDT In_2Se_3 and In_2Se_3 (powder) reference samples. In (b), the Se $M_{4,5}$ XES spectrum of the NaF/KF-PDT CIGSe absorber (dotted blue) is represented by a spectral sum of 0.5 × NaF-PDT CIGSe (red) + 0.5 × KF-PDT In_2Se_3 (gray), resulting in the green spectrum. The difference between data and sum (residual) is also shown. (c) Se $M_{4,5}$ emission of the NaF-PDT and NaF/KF-PDT CIGSe samples, compared to (d) the corresponding "artificial HAXPES-derived XES spectra" (see Figure S7 for more information).

eV[51] and scaled according to the multiplicity (2j+1) (see Figure S7 for more information). The energy scales of the photoemission and X-ray emission measurements are roughly aligned according to the shift between the binding energy of the valence band and the Se 3d core level component Se$_b$ of the NaF/KF-PDT sample. The 8 keV data (IMFP 12 nm[24]) and the Se M$_{4,5}$ XES (effective attenuation length 13 nm[52] for CuInSe$_2$ and KInSe$_2$) data feature similar depth sensitivity, and are, moreover, least affected by surface effects that could impact this approach. The exact shapes of the HAXPES and XES spectra are not expected to be identical due to the different measurement processes involved (e.g., different initial and final states); both types of spectra are related to occupied valence band states, but the relative intensities of the various features are influenced by photoionization cross sections and dipole transition matrix elements. Our comparison therefore focuses on associating the most prominent spectral features (labeled according to ref 11: I′, II′, III′, and V′) with particular electronic states. Note, however, that in contrast to ref 11, here we use Δ_{SO} = 0.83 eV to indicate corresponding spectral regions (instead of a particular E^b). Furthermore, in ref 11, an additional feature IV was attributed to In s/Ga s states[53] that are located at around 7 eV binding energy (roughly corresponding to 46 eV on the emission energy scale, i.e., outside of the measured energy window) and are therefore not displayed in Figure 5c,d.

For the NaF-PDT CIGSe samples, the low binding energy shoulder around I′ (antibonding hybridized Se p−Cu d states,[53] indicated by an arrow) is significantly less pronounced in the (element-specific) Se M$_{4,5}$ X-ray emission (Figure 5c) than in the photoemission spectra (Figure 5d). This is due to its primarily Cu 3d character, which leads to a low transition probability for the Se M$_{4,5}$ XES. As already proposed in ref 11, feature II′ can be ascribed to nonbonding Se p states,[53] and III′ to bonding hybridized Se p−Cu d states.[53] Comparing the spectra for the NaF/KF-PDT CIGSe samples, we can observe a common feature V′ at a binding energy of ∼3 eV that we previously attributed to K 4s derived states.[11] In the XES spectra, the presence of this feature (at ∼50 eV emission energy) is the most significant difference between the NaF/KF-PDT CIGSe and the other samples. As described above, the XES and HAXPES energy axes were aligned using the binding energy of the Se 3d$_{5/2}$ component Se$_b$ of the NaF/KF-PDT sample (that has a similar binding energy as the corresponding Se component of the alkali-free and NaF-PDT CIGSe). The K 4s-derived fluorescence feature in the emission spectrum is, however, related to the Se$_a$ species, and therefore its position in the spectrum is shifted by 0.6 eV—the difference in Se 3d binding energies of Se$_a$ and Se$_b$ (see Figure 1b and Table S2). The presence of this K-related peak in the Se M$_{4,5}$ XES indicates a hybridization between the K and Se states, providing a confirmation of the formation of K—Se bonds and therefore of the incorporation of K into the CIGSe structure. This, in turn, strengthens the suggestion of "the formation of a material containing mainly K, In, and Se" in ref 47.

CONCLUSIONS

We have used quantitative depth-dependent photoelectron spectroscopy, soft X-ray absorption spectroscopy, and soft X-ray emission spectroscopy to study the impact of different alkali postdeposition treatments (PDT) on the near-surface chemical structures of Cu(In,Ga)Se$_2$ (CIGSe) absorbers grown by low-temperature coevaporation. After immersion in aqueous ammonia, we find that the chemical composition of the alkali-free and NaF-PDT CIGSe samples are very similar and indicative of a Cu-poor CIGSe surface structure. In contrast, the core level photoemission spectra and modified Auger parameters of the NaF/KF-PDT CIGSe sample indicate the presence of two distinct compounds, which we ascribe to a K-containing and a K-free species. The composition of the K-free species was determined to be the same as the Cu-poor chalcopyrite surface structure of the alkali-free and NaF-PDT CIGSe absorbers. We identify the K-containing compound as a K—In—Se surface species. This is confirmed by the Se M$_{4,5}$ X-ray emission measurements, which give direct evidence for the formation of Se—K bonds in the NaF/KF-PDT CIGSe sample.

The observed decreasing K and increasing Cu+Ga content of the NaF/KF-PDT CIGSe with increasing bulk sensitivity of the measurement, the similarity of the Cu/(Cu+In$_b$+Ga+Se$_b$) ratio of its primary (K-free) bulk phase to that of the alkali-free and NaF-PDT CIGSe sample, and the identification of two distinct Se and In species for the NaF/KF-PDT CIGSe sample, provide evidence for the formation of a K—In—Se/chalcopyrite bilayer structure as suggested in refs 10 and 11.

The presence of a K—In—Se surface phase on top of the CIGSe absorber results in a completely modified electronic surface structure.[11] Considering the chemical processes (e.g., complex formation) that take place in a chemical bath (i.e., the standard deposition method for the CdS buffer), it can be expected that this modified surface structure will also influence the formation of the buffer/absorber layer interface. In connection with the enhanced efficiency of corresponding solar cell devices, this modified (prospective) interface is interpreted to act as a passivation layer, reducing charge carrier recombination losses at the interface between CdS and CIGSe.

ASSOCIATED CONTENT

Ⓢ Supporting Information

The Supporting Information is available free of charge on the ACS Publications website at DOI: 10.1021/acsami.6b11892.

> XPS/HAXPES survey spectra, dependence of the photoionization cross sections of the orbitals contributing to the CIGSe valence band at different excitation energies, photoemission data with respective Voigt fits for Mg K$_\alpha$ and 2 keV excitation, (In+Ga) and Se ratios, details for the In 4p background subtraction procedure, peak positions for calculating the modified Auger parameter, C K and K L$_{2,3}$ XAS spectra, explanations on the artificial HAXPES-derived XES spectra, and binding energy position of the Se 3d photoemission lines (PDF)

AUTHOR INFORMATION

Corresponding Authors

*E-mail: evelyn.handick@helmholtz-berlin.de (E.H.).
*E-mail: marcus.baer@helmholtz-berlin.de (Ma.B.).

ORCID Ⓘ

Evelyn Handick: 0000-0002-9773-9981

Author Contributions

Several people contributed to the work. E.H., R.G.W., S.B., A.N.T., and Ma.B. designed the basic idea for this work. E.H., P.R., F.P., R.G.W., and Ma.B. planned and/or carried out experiments. D.K.L., Mo.B., L.W., and C.H. (BL8.0.1 of ALS) and D.G., T.C. (BL15XU of SPring-8) participated in the measurements in the framework of joint beamtimes. E.H.,

■ REFERENCES

(1) Jackson, P.; Wuerz, R.; Hariskos, D.; Lotter, E.; Witte, W.; Powalla, M. Effects of Heavy Alkali Elements in Cu(In,Ga)Se2 Solar Cells with Efficiencies up to 22.6%. *Phys. Status Solidi RRL* **2016**, *10* (8), 583−586.

(2) Kamada, R.; Yagioka, T.; Adachi, S.; Handa, A.; Tai, K. F.; Kato, T.; Sugimoto, H. New World Record Cu(In, Ga) (Se, S)2 Thin Film Solar Cell Efficiency beyond 22%. In *2016 IEEE 43rd Photovoltaic Specialists Conference (PVSC)*; 2016; pp 1287−1291.

(3) Jackson, P.; Hariskos, D.; Wuerz, R.; Kiowski, O.; Bauer, A.; Friedlmeier, T. M.; Powalla, M. Properties of Cu(In,Ga)Se2 Solar Cells with New Record Efficiencies up to 21.7%. *Phys. Status Solidi RRL* **2015**, *9* (1), 28−31.

(4) Chirilă, A.; Reinhard, P.; Pianezzi, F.; Bloesch, P.; Uhl, A. R.; Fella, C.; Kranz, L.; Keller, D.; Gretener, C.; Hagendorfer, H.; Jaeger, D.; Erni, R.; Nishiwaki, S.; Buecheler, S.; Tiwari, A. N. Potassium-Induced Surface Modification of Cu(In,Ga)Se2 Thin Films for High-Efficiency Solar Cells. *Nat. Mater.* **2013**, *12* (12), 1107−1111.

(5) Song, X.; Caballero, R.; Félix, R.; Gerlach, D.; Kaufmann, C. A.; Schock, H.-W.; Wilks, R. G.; Bär, M. Na Incorporation into Cu(In,Ga)Se2 Thin-Film Solar Cell Absorbers Deposited on Polyimide: Impact on the Chemical and Electronic Surface Structure. *J. Appl. Phys.* **2012**, *111* (3), 034903.

(6) Zellner, M. B.; Birkmire, R. W.; Eser, E.; Shafarman, W. N.; Chen, J. G. Determination of Activation Barriers for the Diffusion of Sodium through CIGS Thin-Film Solar Cells. *Prog. Photovoltaics* **2003**, *11* (8), 543−548.

(7) Rockett, A.; Granath, K.; Asher, S.; Al Jassim, M. M.; Hasoon, F.; Matson, R.; Basol, B.; Kapur, V.; Britt, J. S.; Gillespie, T.; Marshall, C. Na Incorporation in Mo and CuInSe2 from Production Processes. *Sol. Energy Mater. Sol. Cells* **1999**, *59* (3), 255−264.

(8) Heske, C.; Fink, R.; Umbach, E.; Riedl, W.; Karg, F. Na-induced Effects on the Electronic Structure and Composition of Cu(In,Ga)Se2 Thin-film Surfaces. *Appl. Phys. Lett.* **1996**, *68* (24), 3431−3433.

(9) Wuerz, R.; Eicke, A.; Kessler, F.; Paetel, S.; Efimenko, S.; Schlegel, C. CIGS Thin-Film Solar Cells and Modules on Enamelled Steel Substrates. *Sol. Energy Mater. Sol. Cells* **2012**, *100*, 132−137.

(10) Reinhard, P.; Bissig, B.; Pianezzi, F.; Hagendorfer, H.; Sozzi, G.; Menozzi, R.; Gretener, C.; Nishiwaki, S.; Buecheler, S.; Tiwari, A. N. Alkali-Templated Surface Nanopatterning of Chalcogenide Thin Films: A Novel Approach Toward Solar Cells with Enhanced Efficiency. *Nano Lett.* **2015**, *15* (5), 3334−3340.

(11) Handick, E.; Reinhard, P.; Alsmeier, J.-H.; Köhler, L.; Pianezzi, F.; Krause, S.; Gorgoi, M.; Ikenaga, E.; Koch, N.; Wilks, R. G.; Buecheler, S.; Tiwari, A. N.; Bär, M. Potassium Postdeposition Treatment-Induced Band Gap Widening at Cu(In,Ga)Se2 Surfaces − Reason for Performance Leap? *ACS Appl. Mater. Interfaces* **2015**, *7* (49), 27414−27420.

(12) Laemmle, A.; Wuerz, R.; Powalla, M. Investigation of the Effect of Potassium on Cu(In,Ga)Se2 Layers and Solar Cells. *Thin Solid Films* **2015**, *582*, 27−30.

(13) Muzzillo, C. P.; Mansfield, L. M.; Ramanathan, K.; Anderson, T. J. Properties of Cu1−x K X InSe2 Alloys. *J. Mater. Sci.* **2016**, *51*, 6812−6823.

(14) Chirilă, A.; Buecheler, S.; Pianezzi, F.; Bloesch, P.; Gretener, C.; Uhl, A. R.; Fella, C.; Kranz, L.; Perrenoud, J.; Seyrling, S.; Verma, R.; Nishiwaki, S.; Romanyuk, Y. E.; Bilger, G.; Tiwari, A. N. Highly Efficient Cu(In,Ga)Se2 Solar Cells Grown on Flexible Polymer Films. *Nat. Mater.* **2011**, *10* (11), 857−861.

(15) Briggs, D.; Seah, M. P. *Auger and X-Ray Photoelectron Spectroscopy: Practical Surface Analysis (Appendix 1)*; John Wiley & Sons: Chichester, 1983.

(16) Gorgoi, M.; Svensson, S.; Schäfers, F.; Öhrwall, G.; Mertin, M.; Bressler, P.; Karis, O.; Siegbahn, H.; Sandell, A.; Rensmo, H.; Doherty, W.; Jung, C.; Braun, W.; Eberhardt, W. The High Kinetic Energy Photoelectron Spectroscopy Facility at BESSY Progress and First Results. *Nucl. Instrum. Methods Phys. Res., Sect. A* **2009**, *601* (1−2), 48−53.

(17) Schaefers, F.; Mertin, M.; Gorgoi, M. KMC-1: A High Resolution and High Flux Soft X-Ray Beamline at BESSY. *Rev. Sci. Instrum.* **2007**, *78* (12), 123102.

(18) Ueda, S.; Katsuya, Y.; Tanaka, M.; Yoshikawa, H.; Yamashita, Y.; Ishimaru, S.; Matsushita, Y.; Kobayashi, K. Present Status of the NIMS Contract Beamline BL15XU at SPring-8. In *AIP Conference Proceedings*; AIP Publishing, 2010; Vol. *1234*, pp 403−406.

(19) Ueda, S. Application of Hard X-Ray Photoelectron Spectroscopy to Electronic Structure Measurements for Various Functional Materials. *J. Electron Spectrosc. Relat. Phenom.* **2013**, *190*, 235−241.

(20) Ikenaga, E.; Kobata, M.; Matsuda, H.; Sugiyama, T.; Daimon, H.; Kobayashi, K. Development of High Lateral and Wide Angle Resolved Hard X-Ray Photoemission Spectroscopy at BL47XU in SPring-8. *J. Electron Spectrosc. Relat. Phenom.* **2013**, *190*, 180−187.

(21) Seah, M. P.; Gilmore, I. S.; Beamson, G. XPS: Binding Energy Calibration of Electron Spectrometers 5—re-Evaluation of the Reference Energies. *Surf. Interface Anal.* **1998**, *26* (9), 642−649.

(22) Trzhaskovskaya, M. B.; Nefedov, V. I.; Yarzhemsky, V. G. Photoelectron Angular Distribution Parameters for Elements Z = 1 to Z = 54 in the Photoelectron Energy Range 100−5000 eV. *At. Data Nucl. Data Tables* **2001**, *77* (1), 97−159.

(23) Trzhaskovskaya, M. B.; Nikulin, V. K.; Nefedov, V. I.; Yarzhemsky, V. G. Non-Dipole Second Order Parameters of the Photoelectron Angular Distribution for Elements Z = 1−100 in the Photoelectron Energy Range 1−10 keV. *At. Data Nucl. Data Tables* **2006**, *92* (2), 245−304.

(24) Tanuma, S.; Powell, C. J.; Penn, D. R. Calculations of Electron Inelastic Mean Free Paths. V. Data for 14 Organic Compounds over the 50−2000 eV Range. *Surf. Interface Anal.* **1994**, *21* (3), 165−176.

(25) Jia, J. J.; Callcott, T. A.; Yurkas, J.; Ellis, A. W.; Himpsel, F. J.; Samant, M. G.; Stöhr, J.; Ederer, D. L.; Carlisle, J. A.; Hudson, E. A.; Terminello, L. J.; Shuh, D. K.; Perera, R. C. C. First Experimental Results from IBM/TENN/TULANE/LLNL/LBL Undulator Beamline at the Advanced Light Source. *Rev. Sci. Instrum.* **1995**, *66* (2), 1394−1397.

(26) Handick, E.; Reinhard, P.; Wilks, R. G.; Pianezzi, F.; Félix, R.; Gorgoi, M.; Kunze, T.; Buecheler, S.; Tiwari, A. N.; Bär, M. NaF/KF Post-Deposition Treatments and Their Influence on the Structure of

Cu(In,Ga)Se2 Absorber Surfaces. In *2016 IEEE 43rd Photovoltaic Specialists Conference (PVSC)*; 2016; pp 17−21.

(27) Ghorbani, E.; Kiss, J.; Mirhosseini, H.; Roma, G.; Schmidt, M.; Windeln, J.; Kühne, T. D.; Felser, C. Hybrid-Functional Calculations on the Incorporation of Na and K Impurities into the CuInSe2 and CuIn5Se8 Solar-Cell Materials. *J. Phys. Chem. C* **2015**, *119* (45), 25197−25203.

(28) Morkel, M.; Weinhardt, L.; Lohmüller, B.; Heske, C.; Umbach, E.; Riedl, W.; Zweigart, S.; Karg, F. Flat Conduction-Band Alignment at the CdS/CuInSe2 Thin-Film Solar-Cell Heterojunction. *Appl. Phys. Lett.* **2001**, *79* (27), 4482−4484.

(29) Bär, M.; Nishiwaki, S.; Weinhardt, L.; Pookpanratana, S.; Fuchs, O.; Blum, M.; Yang, W.; Denlinger, J. D.; Shafarman, W. N.; Heske, C. Depth-Resolved Band Gap in Cu(In,Ga)(S,Se)2 Thin Films. *Appl. Phys. Lett.* **2008**, *93* (24), 244103.

(30) Schmid, D.; Ruckh, M.; Grunwald, F.; Schock, H. W. Chalcopyrite/Defect Chalcopyrite Heterojunctions on the Basis of CuInSe2. *J. Appl. Phys.* **1993**, *73* (6), 2902−2909.

(31) Tuttle, J. R.; Albin, D. S.; Noufi, R. Thoughts on the Microstructure of Polycrystalline Thin Film CuInSe2 and Its Impact on Material and Device Performance. *Sol. Cells* **1991**, *30* (1), 21−38.

(32) Liao, D.; Rockett, A. Cu Depletion at the CuInSe2 Surface. *Appl. Phys. Lett.* **2003**, *82* (17), 2829−2831.

(33) McGuire, G. E.; Schweitzer, G. K.; Carlson, T. A. Core Electron Binding Energies in Some Group IIIA, VB, and VIB Compounds. *Inorg. Chem.* **1973**, *12* (10), 2450−2453.

(34) Kazmerski, L. L.; Jamjoum, O.; Ireland, P. J.; Deb, S. K.; Mickelsen, R. A.; Chen, W. Initial Oxidation of CuInSe2. *J. Vac. Sci. Technol.* **1981**, *19* (3), 467−471.

(35) Schmid, D.; Ruckh, M.; Schock, H. W. Photoemission Studies on Cu(In, Ga)Se2 Thin Films and Related Binary Selenides. *Appl. Surf. Sci.* **1996**, *103* (4), 409−429.

(36) Cahen, D.; Ireland, P. J.; Kazmerski, L. L.; Thiel, F. A. X-ray Photoelectron and Auger Electron Spectroscopic Analysis of Surface Treatments and Electrochemical Decomposition of CuInSe2 Photoelectrodes. *J. Appl. Phys.* **1985**, *57* (10), 4761−4771.

(37) Moulder, J. F.; Stickle, W. F.; Sobol, P. E.; Bomben, K. D. *Handbook of X-Ray Photoelectron Spectroscopy*; Perkin-Elmer Corporation: Minnesota, 1992.

(38) Kohiki, S.; Nishitani, M.; Negami, T.; Wada, T. X-Ray Photoelectron Spectroscopy of CuInSe2. *Phys. Rev. B: Condens. Matter Mater. Phys.* **1992**, *45* (16), 9163−9168.

(39) Bahl, M. K.; Watson, R. L.; Irgolic, K. J. LMM Auger Spectra of Selenium and Some of Its Compounds. *J. Chem. Phys.* **1980**, *72* (7), 4069−4077.

(40) Powell, C. J. Recommended Auger-Electron Kinetic Energies for 42 Elemental Solids. *J. Electron Spectrosc. Relat. Phenom.* **2010**, *182* (1−2), 11−18.

(41) Nelson, A. J.; Frigo, S. P.; Rosenberg, R. Valency and Type Conversion in CuInSe2 with H2 Plasma Exposure: A Photoemission Investigation. *J. Appl. Phys.* **1993**, *73* (12), 8561−8564.

(42) Nelson, A. J.; Gebhard, S.; Kazmerski, L. L.; Colavita, E.; Engelhardt, M.; Höchst, H. Formation and Schottky Barrier Height of Au Contacts to CuInSe2. *J. Vac. Sci. Technol., A* **1991**, *9* (3), 978−982.

(43) Ho, C.-H.; Chen, Y.-C. Thickness-Tunable Band Gap Modulation in γ-In2Se3. *RSC Adv.* **2013**, *3* (47), 24896−24899.

(44) Sette, F.; Sinkovic, B.; Ma, Y. J.; Chen, C. T. Crystal-Field Splitting of Core Excitons in Ionic Crystals. *Phys. Rev. B: Condens. Matter Mater. Phys.* **1989**, *39* (15), 11125−11130.

(45) de Groot, F. M. F.; Fuggle, J. C.; Thole, B. T.; Sawatzky, G. A. L2,3 X-Ray-Absorption Edges of d0 Compounds: K+, Ca2+, Sc3+, and Ti4+ in Oh (Octahedral) Symmetry. *Phys. Rev. B: Condens. Matter Mater. Phys.* **1990**, *41* (2), 928−937.

(46) Yanagihara, M.; Maezawa, H.; Sasaki, T.; Iguchi, Y. K+L2,3 Core Level Absorption in Potassium Halides. *J. Phys. Soc. Jpn.* **1985**, *54* (9), 3628−3631.

(47) Reinhard, P.; Bissig, B.; Pianezzi, F.; Avancini, E.; Hagendorfer, H.; Keller, D.; Fuchs, P.; Döbeli, M.; Vigo, C.; Crivelli, P.; Nishiwaki, S.; Buecheler, S.; Tiwari, A. N. Features of KF and NaF Postdeposition Treatments of Cu(In,Ga)Se2 Absorbers for High Efficiency Thin Film Solar Cells. *Chem. Mater.* **2015**, *27* (16), 5755−5764.

(48) D'Addato, S.; Gregory, D. A. C.; Robinson, A. W.; Santaniello, A.; Hellwig, C.; Jung, C.; Evans, D. A. An X-Ray Absorption Spectroscopy Study of the KGaAs(110) Interface. *Solid State Commun.* **1995**, *93* (1), 11−16.

(49) Ma, Y.; Rudolf, P.; Chen, C. T.; Sette, F. Potassium Adsorption on the Si(100)(2 × 1) Surface Studied by Si and K Core Level Photoemission and Photoabsorption Spectroscopy. *J. Vac. Sci. Technol., A* **1992**, *10* (4), 1965−1969.

(50) D'Addato, S.; Ramaker, D. E.; Cosso, R.; Gregory, D.; Morrison, T. P.; Unsworth, P.; Duò, L.; Panaccione, G.; Nannarone, S.; Weightman, P. Charge-Transfer Satellites in K L 23 XAS Data for K/Si(111)-(2 × 1): Evidence for Strong Ionic Bonds. *EPL* **1994**, *26* (2), 85.

(51) Shevchik, N. J.; Cardona, M.; Tejeda, J.; X-Ray. and Far-Uv Photoemission from Amorphous and Crystalline Films of Se and Te. *Phys. Rev. B* **1973**, *8* (6), 2833−2841.

(52) Henke, B. L.; Gullikson, E. M.; Davis, J. C. X-Ray Interactions: Photoabsorption, Scattering, Transmission, and Reflection at E = 50−30,000 eV, Z = 1−92. *At. Data Nucl. Data Tables* **1993**, *54* (2), 181−342.

(53) Kuznetsova, T. V.; Grebennikov, V. I.; Zhao, H.; Derks, C.; Taubitz, C.; Neumann, M.; Persson, C.; Kuznetsov, M. V.; Bodnar, I. V.; Martin, R. W.; Yakushev, M. V. A Photoelectron Spectroscopy Study of the Electronic Structure Evolution in CuInSe2-Related Compounds at Changing Copper Content. *Appl. Phys. Lett.* **2012**, *101* (11), 111607.